Acta Cryst. (1989). B**45**, 1–6

A New Intermetallic Pentagonal Frank–Kasper Phase Determined by HREM*

BY H. Q. YE† AND J. ZHU‡

Beijing Laboratory of Electron Microscopy, Academia Sinica, Beijing, People's Republic of China

(*Received* 8 *December* 1987; *accepted* 25 *April* 1988)

Abstract

A new intermetallic pentagonal Frank–Kasper phase coexisting with the well known μ and Laves phases has been found in precipitates from superalloys. The lattice parameters of the new *PF* phase, which were determined by means of high-resolution electron microscopy and selected-area electron diffraction, are: monoclinic, space group $B2/m$, $a = 20{\cdot}4$, $b = 11{\cdot}7$, $c = 4{\cdot}7$ Å and $\gamma = 112{\cdot}4°$. Based on an analysis of the structural units, the atom positions derived from high-resolution images are also given.

1. Introduction

Structures which contain only interpenetrating coordination polyhedra with 12 (icosahedron), 14, 15 or 16 vertices and triangulate faces are filled in space by a somewhat distorted tetrahedral packing of the atoms. A systematic treatment of these tetrahedrally close-packed (t.c.p.) phases has been given by Frank & Kasper (1958, 1959), who argued that there is no CN13 coordination shell and no regular shells with CN > 16 in these structures. Therefore, the layered structures containing only interpenetrating CN12, 14, 15 or 16 polyhedra are referred to as Frank–Kasper (*FK*) phases. Somewhat later, Shoemaker & Shoemaker (1969) classified these t.c.p. structures according to the main polygons in the primary layer, giving three categories: hexagons, pentagons and a mixture of the two. Recently, Andersson (1978) pointed out that complex t.c.p. phases can be visualized as consisting of simple elementary structural units. Therefore they form a hierarchy of structures from simple to complex, and a systematic classification of these phases has been presented according to different-order structures (Kuo, Ye & Li, 1986).

The *FK* phases precipitated in superalloys may markedly degrade the plasticity and toughness of the superalloys: thus many X-ray and electron diffraction investigations have been carried out in the last 30 years, but few new phases have been discovered. Thanks to the recent development of HREM to the level of atomic resolution, defects in these structures have become the subject of study in many high-resolution electron microscopy laboratories. For instance, long-period structures in the Laves phase (Komura, Takeda & Takata, 1983) and planar faults in the μ phase (Hiraga, Yamamoto & Hirabayashi, 1983) have been studied. However, these investigations were made using samples of intermetallic phases specially melted from pure metals with rather simple compositions at the equilibrium state. This differs from the t.c.p. phases precipitated in superalloys of varied composition. The microstructures of *FK* phases in superalloys have been extensively studied at the atomic level with HREM and SAED in the Laboratory of Atomic Imaging of Solids and six new phases, namely, *H* (Ye, Li & Kuo, 1984), *F*, *K*, *J* (Li & Kuo, 1986) and *C*, *C*1 (Wang, Ye & Kuo, 1986), and a magnitude of microdomain structures have been found (Kuo, Ye & Li, 1986). The small size, in general less than 0·1 μm, and the small amounts of these phases may be the main reasons why they could not be detected in the past by X-ray diffraction. The merits of HREM can be fully utilized in such studies.

For the pentagonal *FK* (*PFK*) phases in which icosahedra play a dominant role, although ideal tetrahedra cannot pack together to fill space completely and a somewhat distorted tetrahedral packing of the atoms cannot be avoided, the misfit is at least relatively small for the icosahedra. The *PFK* structures are in most cases generated by the alternate stacking of primary layers of pentagonal–triangular nets of atoms with secondary layers of triangular–rectangular nets of atoms. The normal line of such stacking layers coincides with the common fivefold axis of icosahedral columns or pentagonal antiprisms. The rather remarkable geometrical properties of the *PFK* phases make them easy to classify and describe by means of a code which represents the configurations of juxtaposition of the simplest structural units, $MgCu_2$ (triangle) and Zr_4Al_3 (rectangle) (Shoemaker & Shoemaker, 1972; Kuo, Ye & Li, 1986; Ye, 1987). Their HREM images, in which each bright dot corresponds to a tunnel inside the icosahedral column, can therefore be considered as the projected images of metal atoms in the centre of icosahedral columns (Ye, Li & Kuo, 1985; Ye, Wang & Kuo, 1985; Wang, Ye & Kuo, 1986). Combining the

* Project supported by National Nature Science Foundation of China.

† Also at the Laboratory of Atomic Imaging of Solids, Academia Sinica, 110015 Shenyang, People's Republic of China.

‡ Also at Central Iron and Steel Research Institute, 100081 Beijing, People's Republic of China.

0108-7681/89/010001-06$03.00

Table 1. *Parameters used for image simulation*

Acceleration voltage (kV)	250
Spherical-aberration coefficient (mm)	1·2
Incident-beam divergence (mrad)	1
Half-width of defocus spread due to chromatic aberration (Å)	130
Objective aperture (Å^{-1})	0·35
Crystal thickness for one slice (Å)	4·7

HREM image and selected-area electron diffraction pattern, the lattice and unit-cell parameters of an unknown *PFK* phase may be determined. In this work, a new intermetallic *FK* phase with juxtaposed icosahedral columns, called the *PF* phase here, was found coexisting with the μ phase.

2. Experimental

The Ni-based superalloy used in the present investigation has the following composition (wt%) determined by chemical analysis:

Cr	Ni	Mo	Al	Ti	B	Fe
13·0	42·5	6·0	0·35	2·35	0·01	Balance

After heating to 1423 K for 4 h followed by ageing at 973 K for 3000 h, the μ phase was extracted electrolytically from this alloy. The crystallites were collected on a holey carbon film supported on a copper grid. The high-resolution observations were performed with a Philips 430 electron microscope. Composition analysis of the precipitates was carried out on an electron probe.

The computer image simulation was carried out using the multislice program written by Ishizuka (1982) including first- and second-order partial coherent envelopes. The parameters used in the calculations are given in Table 1. The variation in the statistically independent fluctuations in accelerating voltage and objective current, *i.e.,* the half-width of a Gaussian spread of defocus, is 130 Å at the experimental gun bias. The semiangle of convergence of the incident beam, $\theta_c = 1$ mrad, can be estimated from a focused condenser aperture diffraction pattern. The size limited by objective aperature $(\sin\theta/\lambda) = 0{\cdot}35$ Å^{-1}, can be measured from a double-exposed diffraction pattern, and within the objective aperture 457 reflections were chosen and stored in order to calculate the images. The main factors affecting the image are the crystal thickness and defocus values, which may be estimated from the *Pendellösung* dark band for the former and from the width of Fresnel fringe outside the edge of crystal for the latter. In our image simulation, a series of thicknesses and defocus values was chosen.

3. Structure determination

Fig. 1 is a general view of domain structures of the new phase in the precipitates. Around the configuration of the *C*15 Laves phase, which forms a hexagon with the two long sides opposite the 72° vertical angles, two Zr_4Al_3 units are attached to the long sides of the hexagon with the other two Zr_4Al_3 units joined to the opposite short sides. The remaining short sides could only be connected with $MgCu_2$ units in order to fill a plane. Fig. 2(*a*) shows such an arrangement of the structural blocks. This shape of cluster in the secondary layer of *PFK* phases is an analogue of 3^6 configuration with six Cr_3Si units joined in juxtaposition of hexagonal antiprisms in the hexagonal *FK* phases, such as in the *F*, *K* phases (Li & Kuo, 1986). From the outlined hexagonal nodes a new *FK* structure could be detected.

Fig. 3 shows the new phase coexisting with the μ and Laves phases. Since each bright dot in the image of the μ and Laves phases is known with certainty to represent an icosahedral column (Ye, Li & Kuo, 1985), the bright dots in this new structure may also have the same interpretation and some $MgCu_2$ and Zr_4Al_3 units are outlined in the image as well as in a schematic diagram (Fig. 2*b*). Because the configuration of the juxtaposed icosahedral columns in this phase is similar to the $3^6 + 33434$ (1:6) network of the hexagonal *F* phase (Fig. 2*c*), this phase was named as the pentagonal *F*

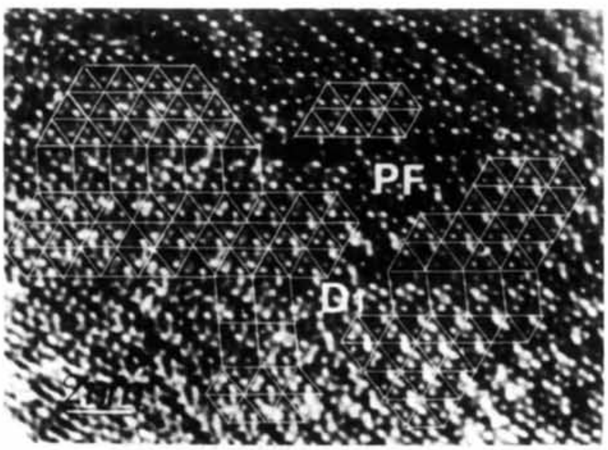

Fig. 1. General mosaic appearance of the *PF* domain structure; the projected units of the *PF* phase and *D*1 structure are outlined.

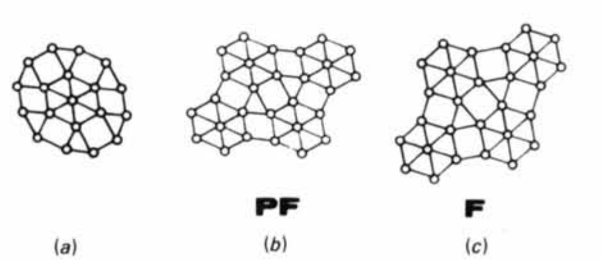

Fig. 2. Schematic diagrams of the ellipse-like cluster of icosahedral columns (*a*), the configuration of the juxtaposed pentagonal antiprisms in the *PF* phase (*b*) and the network of the juxtaposed hexagonal antiprisms in the *F* phase (*c*). Each dot represents a central atom in the tunnel of pentagonal and hexagonal antiprisms.

(*PF*) phase. The corresponding selected-area electron diffraction pattern (EDP) usually showed a composite pattern of the *PF*, μ and Laves phases. However, the EDP of a *PF* single crystal could be observed frequently in the thicker region of the specimen. From such selected-area electron diffraction patterns (Fig. 4), a projected monoclinic unit cell with dimensions $10{\cdot}2 \times 11{\cdot}7$ Å and $\gamma = 112°$ could be defined. The lattice parameters of the new phase derived from the experimental data should be $a = 10{\cdot}2$, $b = 11{\cdot}7$, $c = 4{\cdot}7$ Å and $\gamma = 112°$. Their refinement depends upon a careful geometrical analysis of the projected structural model based on certain assumptions.

Fig. 5 is a schematic illustration of the positions of atoms at the centre of the icosahedral columns in the (001)-projected plane of the *PF* phase. When all the atoms located at the periphery of an icosahedral column are considered, the $Z1$ and $Z2$ units are shifted by $c/2$. The unit cell of the *PF* phase, therefore, has to be B-centred. The basic vectors of the Zr_4Al_3 and $MgCu_2$ units, *i.e.* **X**, **Y**, **Z** and **X**, **W**, **Z**, respectively, are also shown in Fig. 5. The length of the short side in both structural units (Y and W) is about 4 Å in the high-resolution images of the intermetallic μ and Laves phases. Thus, the long sides (X) should be $4{\cdot}7$ Å according to the geometrical relation in the $MgCu_2$ triangle. In other words, $X = Z = 4{\cdot}7$, $Y = W = 4$ Å and $\gamma = 54°$. All atom positions x, y and z in the **X**, **Y**, **Z** or **X**, **W**, **Z** systems can be found in reference texts (for example, Pearson, 1972). From Fig. 5, the lattice parameters can be derived as $a = 4(p + q) = 4(X/2 + W\sin 54°) = 20{\cdot}4$ Å, $b = 2DE = 2(X^2 + Y^2)^{1/2}\cos s = 2(X^2 + Y^2)^{1/2}\cos[(\pi/2 - 54°)/2] = 11{\cdot}7$ Å, $c = 4{\cdot}7$ Å, $\gamma = \pi - \varepsilon - s = 112{\cdot}4°$ and the total number of atoms in the unit cell is 88.

In order to calculate the atom positions in the PF system (**a**, **b**, **c**), it is better to introduce a normalized right-angle system **i**, **j**, **k** with **j**∥**b**, **k**∥**c**, **i**∥**j** × **k** and $i = X = Z$. Moreover, five reference vectors $\mathbf{e}_1$, $\mathbf{e}_2$, $\mathbf{e}_3$, $\mathbf{e}_4$ and $\mathbf{e}_5$ are defined in the **ijk** system in order to describe the position vectors $\mathbf{r}_n$ of the icosahedral columns. An atom at (X_{PF}, Y_{PF}, Z_{PF}) with respect to a coordinate system defined by **a**, **b** and **c** is given by two vectors (r_{nx}, r_{ny}, r_{nz}) and (x_T, y_T, z_T), where T represents the orthonormal coordinate system **i**, **j**, **k**. Therefore, the atom positions in the *PF* system (**a**, **b**, **c**) may be defined by the following equation:

$$(x_{PF} y_{PF} z_{PF}) = \{(x_T y_T z_T)\,[T] + (r_{nx} r_{ny} r_{nz})\}\,[A]^{-1}.$$

Definitions of matrices $[T]$ and $[A]$, and the calculation process are presented in the *Appendix*. The atom coordinates of the *PF* phase are listed in Table 2.

The (001)-projected structural model is shown in Fig. 6, where circles of different size represent atoms with different CN's except the atoms at the centre of the icosahedral columns which are always occupied by CN12 but are drawn as double circles so that they can be distinguished from atoms in primary layers. In Fig. 6 the networks with real or dotted lines indicate the height of the atoms. An image simulation based upon the

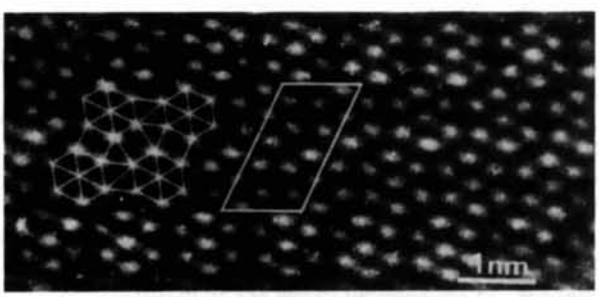

Fig. 3. [001] HREM image of the *PF* phase with a unit cell and the configuration of the building blocks outlined.

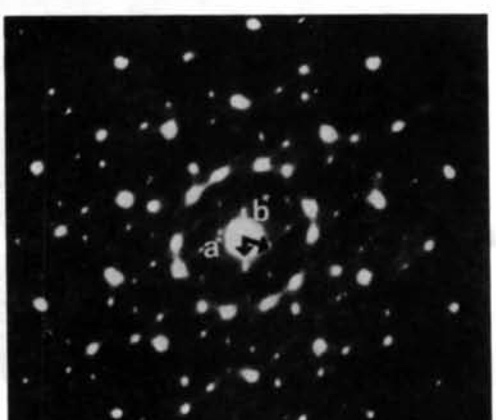

Fig. 4. [001] Zone electron diffraction pattern of the *PF* phase.

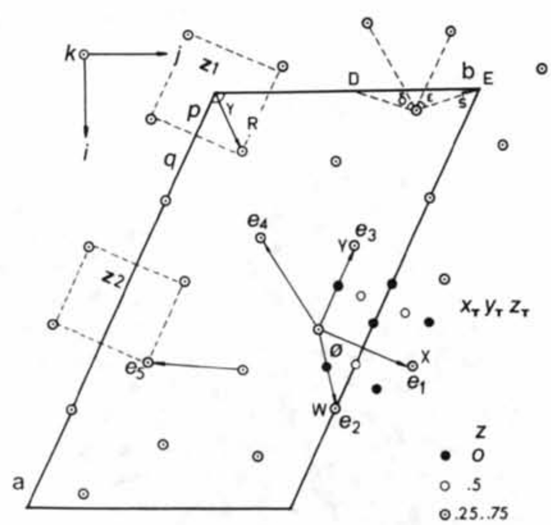

Fig. 5. Schematic illustration of the positions of the atoms at the centre of the icosahedral columns in the (001)-projected plane of the *PF* phase. Several reference coordinate systems used in a geometrical analysis to define the atom positions are also shown.

Table 2. *Crystal structure data of the monoclinic phase system, space group B*2/*m*

$a = 20{\cdot}4$, $b = 11{\cdot}7$, $c = 4{\cdot}7$ Å, $\beta = 112{\cdot}4°$

Position	Atomic species	x	y	z	CN	CN%
(000)+; ($\frac{1}{2}$0$\frac{1}{2}$)+						
4(*e*)	4Fe	0·250	0·000	0·250	12	
		0·750	0·000	0·250	12	
($xy0$); ($\overline{xy}0$)						
4(i)	4Fe	0·350	0·108	0·000	12	
	4Fe	0·546	0·217	0·000	12	
	4Fe	0·397	0·325	0·000	12	
	4Fe	0·695	0·108	0·000	12	
	4Fe	0·742	0·325	0·000	12	
	4Fe	0·150	0·392	0·000	12	
(xyz); ($\overline{xy}z$); ($\overline{xyz}$); ($xy\bar{z}$)						
8(*j*)	8Fe	0·142	0·217	0·250	12	
	8Fe	0·451	0·217	0·250	12	
	8Fe	0·343	0·433	0·250	12	59
4(i)	4Mo	0·025	0·118	0·000	14	
	4Mo	0·944	0·405	0·000	14	9
	4Mo	0·440	0·000	0·000	15	
	4Mo	0·534	0·432	0·000	15	9
	4Mo	0·075	0·349	0·000	16	
	4Mo	0·133	0·000	0·000	16	
	4Mo	0·259	0·217	0·000	16	
	4Mo	0·224	0·432	0·000	16	
	4Mo	0·834	0·217	0·000	16	23

calculated atom positions was carried out and typical results are shown in Fig. 7. The appearance of the image changes rapidly with defocus value and thickness of the crystal. The bright spots forming a $(\underline{3}33)2 + 4\underline{3}3^3 + 43^5 + 434\underline{3}3$ (1:2:2:2) network in the simulated image for the *PF* phase can be obtained in the thickness range 25–70 Å at optimum defocus (−514 Å) as well as some reverse Scherzer defocus.

The chemical composition of the *PF* phase is still unknown. The coexisting μ phase has the composition $Fe_{32}Ni_8Cr_{16}Mo_{22}Al_{24}Ti_6$. In our image simulation, we have tentatively assumed that the *PF* phase may have the simple composition $Fe_{52}Mo_{36}$ in which Fe atoms occupy the CN12 positions with Mo placed at the CN14, 15 or 16 positions. Because the electron-scattering factors of Fe, Ni and Cr atoms are almost the same, the above assumption may not cause serious errors in the dynamic diffraction calculation.

4. Discussion

Another phase with the pentagonal σ structure was also observed. Fig. 8 shows its [001] diffraction pattern where the outermost ten intense diffraction spots are easily recognized. The (330) and (410) diffraction spots have strong intensities which are similar to those of the hexagonal σ phase, but the intensities of (040) are stronger than those of (140). These make its diffraction pattern distinct. Moreover, the known pentagonal σ phase is orthorhombic with composition $W_6(Fe,Si)_7$ or Th_6Cd_7 (Shoemaker & Shoemaker, 1986). The chemical composition of the pentagonal σ phase found in our specimen is unknown. It is reasonable to assume that this phase is probably intermetallic rather than a silicide, since it always occurs in intimate intergrowth with μ and Laves phases. Although we were unable to obtain a high-resolution image of the pentagonal σ phase corresponding to Fig. 8 because the crystal was too thick, the configuration of the pentagonal σ phase and its microdomains were frequently observed in the high-resolution images of the complex domain structures (Fig. 9).

Some more complex structures, mainly built up from the ellipse-like configuration (Fig. 2*a*) and two elementary structural units, were observed in the specimens. Fig. 10 is a schematic diagram of two derivative *PF*-related structures *D*1 and *D*2 representing the networks of their secondary layers. Although no diffraction patterns of these derivative structures have been obtained, small regions of these structures can easily be identified in the high-resolution electron micrograph. Fig. 1 shows two slabs of the *D*1 structure and Fig. 11 the domain of the *D*2 structure.

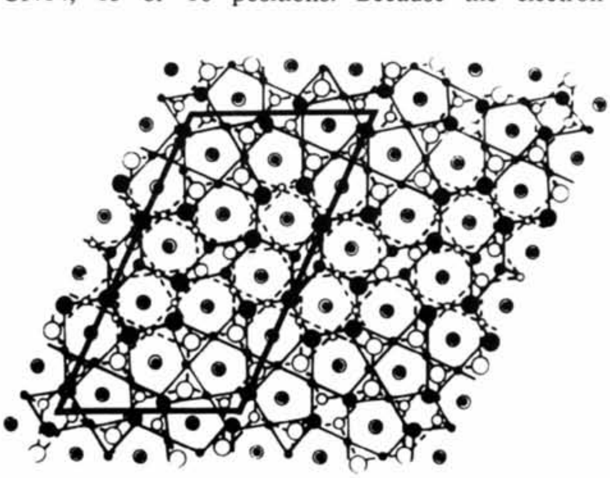

Fig. 6. [001]-Projected structural model of the *PF* phase with a unit cell outlined.

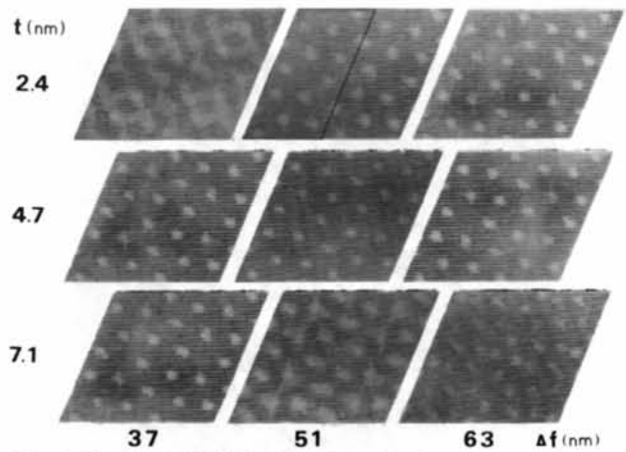

Fig. 7. Simulated [001] images of the *PF* phase over a thickness range of 24 to 71 Å at defocus values of −370, −514 and −632 Å, respectively.

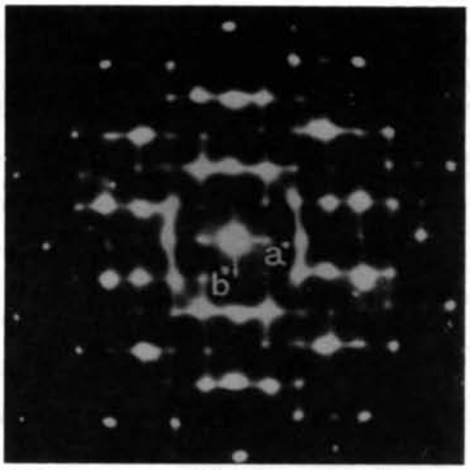

Fig. 8. [001] Zone electron diffraction pattern of the pentagonal σ phase.

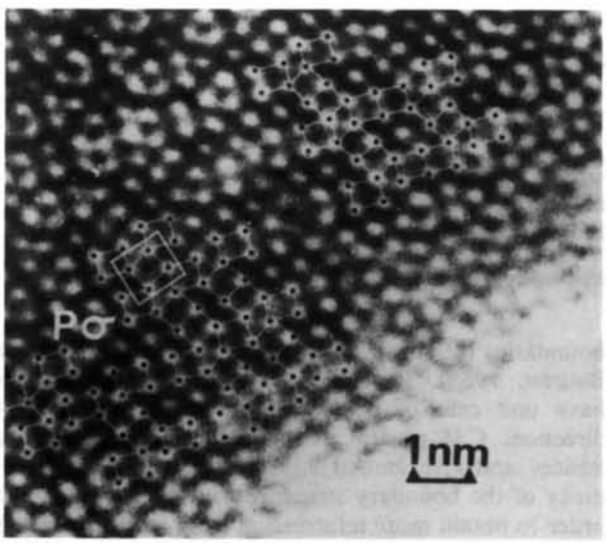

Fig. 9. High-resolution image of microdomains of the pentagonal σ phase with an outlined rectangular unit cell.

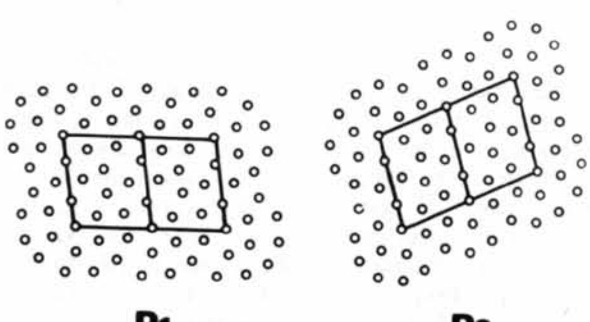

Fig. 10. Schematic diagrams of two derivative *PF*-related structures *D*1 and *D*2. Each dot represents an icosahedral column and the centre of the ellipse-like cluster of these icosahedral columns is outlined.

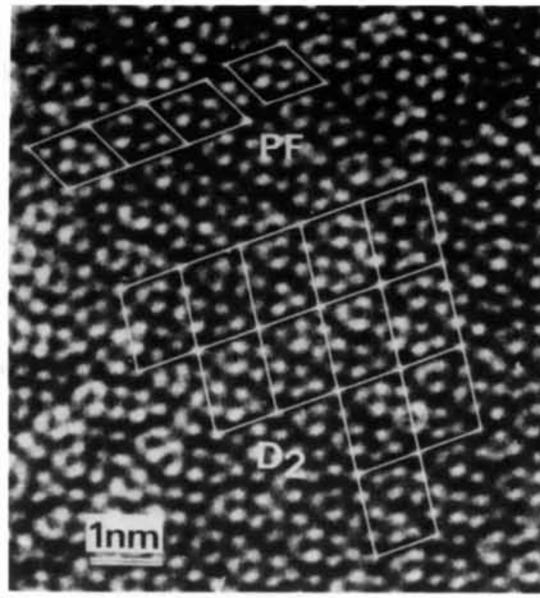

Fig. 11. High-resolution image of the microdomain of the *D*2 structure.

APPENDIX

We have the relations

$$(\mathbf{abc}) = (\mathbf{ijk})\,[A],$$

where

$$[A] = \begin{pmatrix} a\sin\gamma & 0 & 0 \\ a\cos\gamma & b & 0 \\ 0 & 0 & 0 \end{pmatrix}$$

and

$$(\mathbf{ijk}) = (\mathbf{abc})\,[A]^{-1}.$$

If the atom coordinates within the *n*th structural unit are known as x_T, y_T and z_T, and the $\mathbf{a}_{Tn}$, $\mathbf{b}_{Tn}$ and $\mathbf{c}_{Tn}$ coordinate axes of the *n*th structural unit, which define the orientation of the unit, are expressed by the $\mathbf{e}_i$ vectors, we also have

$$(\mathbf{a}_{Tn}\mathbf{b}_{Tn}\mathbf{c}_{Tn}) = (\mathbf{ijk})\,[Tn],$$

where

$$[Tn] = \begin{pmatrix} e_{ix} & e_{jx} & 0 \\ e_{iy} & e_{jy} & 0 \\ e_{iz} & e_{jz} & c \end{pmatrix}.$$

From the identical equation

$$(x_T y_T z_T)\begin{pmatrix} \mathbf{a}_{Tn} \\ \mathbf{b}_{Tn} \\ \mathbf{c}_{Tn} \end{pmatrix} = (x_i y_j z_k)\begin{pmatrix} \mathbf{i} \\ \mathbf{j} \\ \mathbf{k} \end{pmatrix} = (x_{PF} y_{PF} z_{PF})\begin{pmatrix} \mathbf{a} \\ \mathbf{b} \\ \mathbf{c} \end{pmatrix}$$

we obtain

$$(x_{PF} y_{PF} z_{PF}) = (x_T y_T z_T)\,[T]\,[A]^{-1}.$$

Before operating on the matrix $[A]^{-1}$, the $\mathbf{r}_n$ vector (in the **ijk** system), which defines the positions of the nth structural unit, should be added to the $(x_T y_T z_T)$ $[T]$ vector. So that the final formula is

$$(x_{PF} y_{PF} z_{PF}) = \{(x_T y_T z_T)[T] + (r_{nx} r_{ny} r_{nz})\}[A]^{-1}.$$

References

ANDERSSON, S. (1978). *J. Solid State Chem.* **23**, 191–204.
FRANK, F. C. & KASPER, J. S. (1958). *Acta Cryst.* **11**, 184–196.
FRANK, F. C. & KASPER, J. S. (1959). *Acta Cryst.* **12**, 483–499.
HIRAGA, K., YAMAMOTO, T. & HIRABAYASHI, M. (1983). *Trans. Jpn Inst. Met.* **24**, 421–430.
ISHIZUKA, K. (1982). *Acta Cryst.* A**38**, 773–779.
KOMURA, Y., TAKEDA, S. & TAKATA, M. (1983). *Trans. Jpn Inst. Met.* **24**, 315–322.
KUO, K. H., YE, H. Q. & LI, D. X. (1986). *J. Mater. Sci.* **21**, 2597–2622.
LI, D. X. & KUO, K. H. (1986). *Acta Cryst.* B**42**, 152–159.
PEARSON, W. B. (1972). *The Crystal Chemistry and Physics of Metals and Alloys*. New York: Wiley–Interscience.
SHOEMAKER, D. P. & SHOEMAKER, C. B. (1969). *Developments in the Structural Chemistry of Alloy Phases*, pp. 107–139. New York: Plenum.
SHOEMAKER, D. P. & SHOEMAKER, C. B. (1972). *Acta Cryst.* B**28**, 2957–2965.
SHOEMAKER, D. P. & SHOEMAKER, C. B. (1986). *Acta Cryst.* B**42**, 3–18.
WANG, D. N., YE, H. Q. & KUO, K. H. (1986). *Acta Cryst.* B**42**, 21–25.
YE, H. Q. (1987). *J. Electron Microsc. Tech.* **7**, 283–292.
YE, H. Q., LI, D. X. & KUO, K. H. (1984). *Acta Cryst.* B**40**, 461–465.
YE, H. Q., LI, D. X. & KUO, K. H. (1985). *Philos. Mag.* **51**, 829–837.
YE, H. Q., WANG, D. N. & KUO, K. H. (1985). *Philos. Mag.* **51**, 839–848.

Acta Cryst. (1989). B**45**, 6–13

Grain Boundary Structure Analysed by a Coincidence-Site-Lattice Pattern for a Layer Stacking Structure of the 4*H*-Type Laves Phase

BY M. TAKATA, Y. KITANO AND Y. KOMURA

Department of Materials Science, Faculty of Science, Hiroshima University, Higashi-senda-machi, Naka-ku, Hiroshima 730, Japan

(*Received* 15 *May* 1987; *accepted* 20 *July* 1988)

Abstract

A coincidence-site-lattice (CSL) model is applied to the 4*H*-type layer stacking structure of $Mg(Cu,Al)_2$ alloys of the Laves phase, in order to analyse the structure of densely packed plane (DPP) boundaries which are observed by high-resolution electron microscopy (HREM). In this analysis 'lattice point' is used in a wide sense, including all the origins of the repeating unit in every layer. Owing to this extension, extra coincidence sites of lattice points (CSL-points) occur in the interpenetrating lattices and produce a characteristic pattern which is called a CSL-pattern in this paper. The CSL-pattern gives a satisfactory model for the boundary structure of layer stacking structures such as the Laves phase. Basis vectors of the displacement-shift-complete (DSC) lattice obtained here are smaller than those of the usual DSC-lattice and explain well the Burgers vectors of grain boundary dislocations (GBD's). Step vectors and step heights associated with the GBD's are also discussed in detail for the DPP-boundary.

1. Introduction

It has been verified by HREM that the CSL-model is useful for investigations of repeating structures of grain boundaries (Ichinose & Ishida, 1981; d'Anterroches & Bourret, 1984). Since most layer stacking structures have unit cells of considerable size in the stacking direction, CSL-points are sparse in interpenetrating lattices and give limited information about the periodicity of the boundary structure with a long period. In order to obtain more information from interpenetrating lattices, we adopt all the origins of the repeating unit in every layer as 'lattice points' when drawing the interpenetrating lattices. This extension of 'lattice point' is applied to the 4*H* structure of the Laves phase to analyse the boundary structure.

The Laves phase is one of the intermetallic compounds having tetrahedrally close-packed structures. But the crystal structure of the Laves phase is simply understood to be a layer stacking structure of basal planes (Komura, 1962), where one layer is composed of four densely packed atomic planes and is called a fundamental layer of the Laves phase. For example, three basic structures of the Laves phase, $MgZn_2$-(C14)-type (Friauf, 1927*a*), $MgCu_2$(C15)-type (Friauf, 1927*b*) and $MgNi_2$(C36)-type (Laves & Witte, 1935), are illustrated in Fig. 1, where each drawing is divided into two, three or four fundamental layers by dotted lines. In a unit cell of the C14 structure two fundamental layers stack similar to the h.c.p. layer sequence,

0108-7681/89/010006-08$03.00